Figure S1

A

Bottom surface of lens in histology, colored separately across multiple histological planes (*n* = 13)
Lenses biased towards the anterior part of the cortical amygdala (*n* = 6)
Lenses biased towards the posterior part of the cortical amygdala (*n* = 7)

500 µm

AP: -1.22   AP: -1.46   AP: -1.70   AP: -1.94   AP: -2.18   AP: -2.54

B

anterior pICoA
AP: -1.58

posterior pICoA
AP: -2.06

lens

C

1 mV   TMT
1 mV   4MT
1 mV   IAA
1 mV   Hep
0.5 mV   Peanut
1 mV   2PE

trial number
2 4 6 8 10 12 14 16 18 20

D

TMT   IAA   Peanut
4MT   Heptanol   2PE

Mean PID (mV)
Trial number

E

TMT   IAA   2PE

Trial number
Time from odor (S)
ΔF/F

F

TMT   IAA   Peanut
4MT   Heptanol   2PE

Counts
Number of trials that neurons respond to odor (responsive neurons only)

G

ranked subacc.
shuffled
highest   lowest

H

— data average
✕ lin. fit (BIC= -67.0)
✕ exp. fit (BIC= -316)

Percent subacc. > 95th shuffled
sorted rank

I

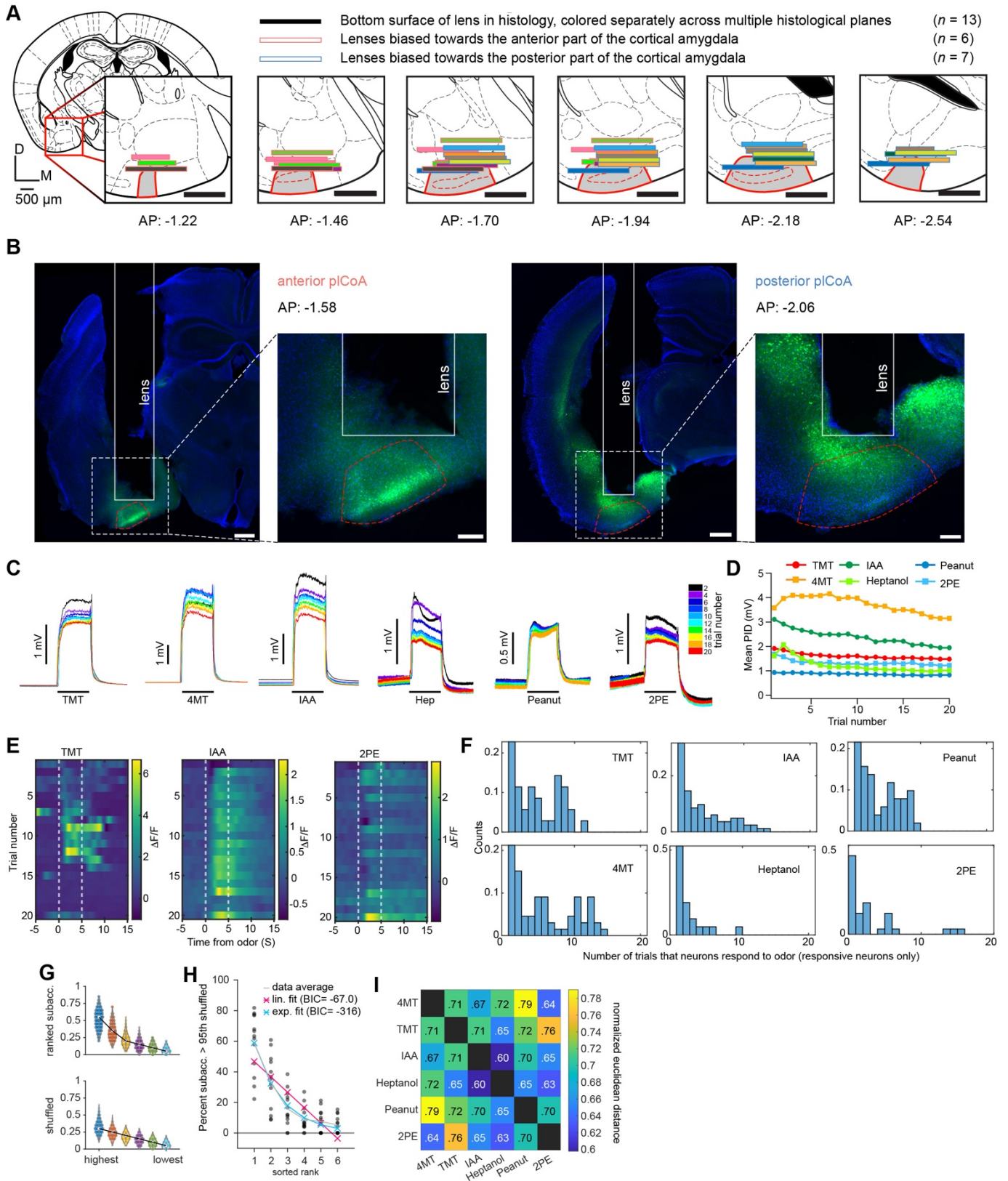|	4MT	TMT	IAA	Heptanol	Peanut	2PE
4MT		.71	.67	.72	.79	.64
TMT	.71		.71	.65	.72	.76
IAA	.67	.71		.60	.70	.65
Heptanol	.72	.65	.60		.65	.63
Peanut	.79	.72	.70	.65		.70
2PE	.64	.76	.65	.63	.70	

normalized euclidean distance

Figure S1. Additional information for imaging experiments. Related to **Figure 1.**

(**A**) Histologically verified placements for GRIN lenses (bars) in wild type animals infected with AAV-hSyn-GCaMP8s for calcium imaging experiments. Horizontal lines indicate locations where lens placements were visible in coronal sections at various positions in the plCoA anterior-posterior axis. Different color bars represent placements in each of 13 animals. Those scored as anterior are outlined in red, and those in posterior are outlined in blue.

(**B**) Histology for anterior plCoA (left) and posterionr plCoA (right) lens implant and jGCaMP8s (green) viral injection sites in representative animals. Scale bar for full size images, 500 μm; scale bar for magnified images, 200 μm.

(**C**) PID recordings across 20 trials for each odor skipping every other one. Trials are colored according to odor. The odor bar indicates 5 seconds.

(**D**) The average PID signal during the odor on period for each odor as a function of trial number. In calculation of the mean, the baseline was offset to approximately zero for each odor, to adjust for drift in the recordings over time.

(**E**) Representative peristimulus time heatmaps of single neuron responses across trials. Each plot is for one neuron in response to one odor. Odor period between 0-5 seconds, marked by white dashed lines.

(**F**) Histograms reporting the distribution for the number of trials neurons respond to each odor. Neurons were considered responsive with a $Z > 2$.

(**G**) Ranked sub-accuracies for single-neuron MNR classifiers (Figure 1L) in violin plots for those trained on real (top) or shuffled (bottom) data. Black lines connect the median across each rank.

(**H**) Scatter plot of percentage of sub-accuracies above the 95th percentile of the shuffled controls for each animal plotted against the rank of the sub-accuracy. Red and blue lines show the linear and exponential fit, respectively, and a gray dashed line connects data averages.

(**I**) Heatmap of the normalized average pairwise Euclidean distance of odor response vectors across biological replicates.
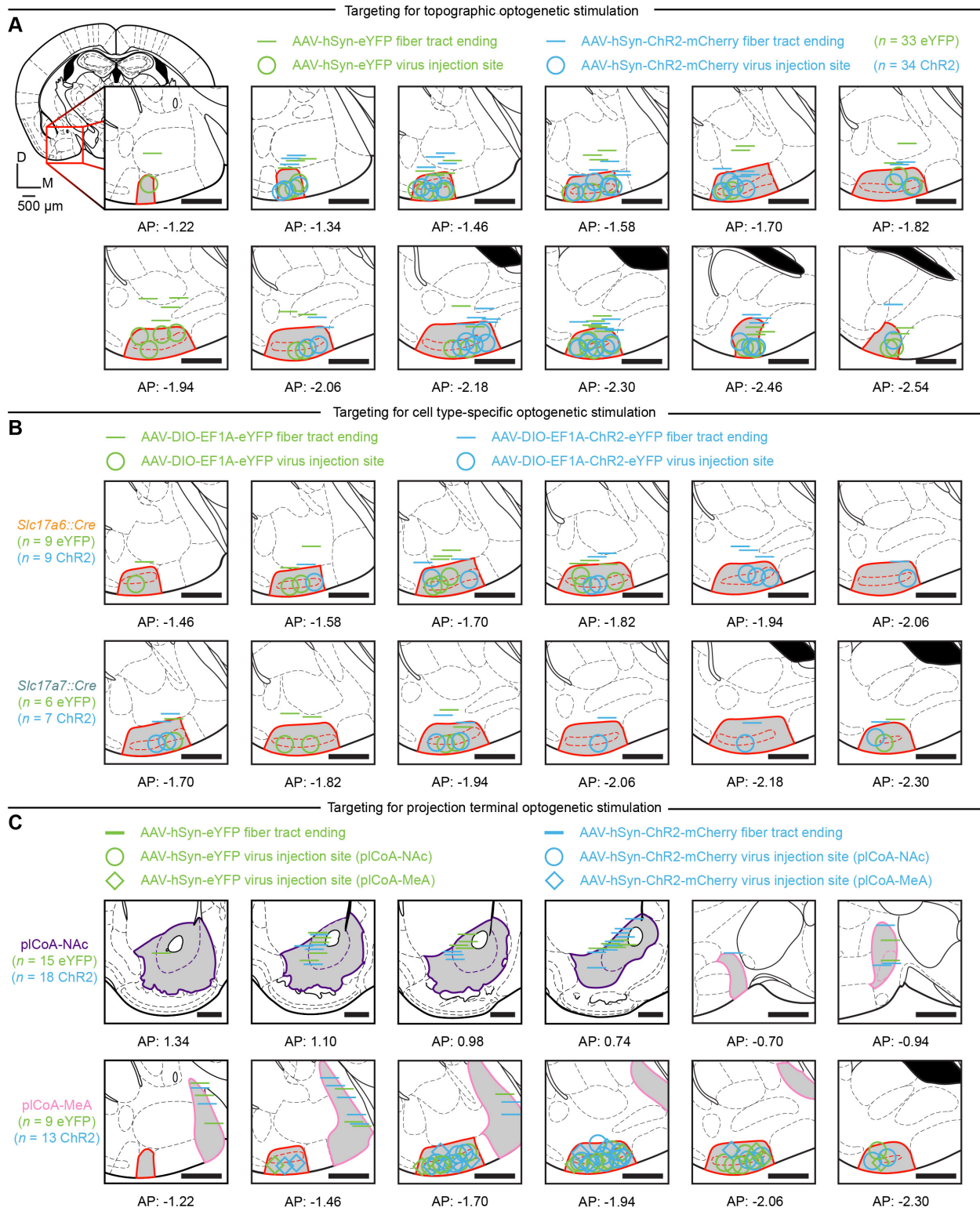
Figure S2

A — Targeting for topographic optogenetic stimulation

— AAV-hSyn-eYFP fiber tract ending
○ AAV-hSyn-eYFP virus injection site

— AAV-hSyn-ChR2-mCherry fiber tract ending (*n* = 33 eYFP)
○ AAV-hSyn-ChR2-mCherry virus injection site (*n* = 34 ChR2)

500 µm

AP: -1.22   AP: -1.34   AP: -1.46   AP: -1.58   AP: -1.70   AP: -1.82

AP: -1.94   AP: -2.06   AP: -2.18   AP: -2.30   AP: -2.46   AP: -2.54

B — Targeting for cell type-specific optogenetic stimulation

— AAV-DIO-EF1A-eYFP fiber tract ending
○ AAV-DIO-EF1A-eYFP virus injection site

— AAV-DIO-EF1A-ChR2-eYFP fiber tract ending
○ AAV-DIO-EF1A-ChR2-eYFP virus injection site

Slc17a6::Cre
(*n* = 9 eYFP)
(*n* = 9 ChR2)

AP: -1.46   AP: -1.58   AP: -1.70   AP: -1.82   AP: -1.94   AP: -2.06

Slc17a7::Cre
(*n* = 6 eYFP)
(*n* = 7 ChR2)

AP: -1.70   AP: -1.82   AP: -1.94   AP: -2.06   AP: -2.18   AP: -2.30

C — Targeting for projection terminal optogenetic stimulation

— AAV-hSyn-eYFP fiber tract ending
○ AAV-hSyn-eYFP virus injection site (plCoA-NAc)
◇ AAV-hSyn-eYFP virus injection site (plCoA-MeA)

— AAV-hSyn-ChR2-mCherry fiber tract ending
○ AAV-hSyn-ChR2-mCherry virus injection site (plCoA-NAc)
◇ AAV-hSyn-ChR2-mCherry virus injection site (plCoA-MeA)

plCoA-NAc
(*n* = 15 eYFP)
(*n* = 18 ChR2)

AP: 1.34   AP: 1.10   AP: 0.98   AP: 0.74   AP: -0.70   AP: -0.94

plCoA-MeA
(*n* = 9 eYFP)
(*n* = 13 ChR2)

AP: -1.22   AP: -1.46   AP: -1.70   AP: -1.94   AP: -2.06   AP: -2.30

Figure S2. Targeting of plCoA neurons for optogenetic stimulation. Related to **Figures 2**, **5**, **7**, **S3**, and **S8**.
(**A**) Histologically verified placements for optic fiber implants (bars) and viral injection sites (circles) in wild type animals infected with AAV-hSyn-ChR2-mCherry (blue) or AAV-hSyn-eYFP (green) in topographic optogenetic cell body stimulation experiments in **Figure 1** and **S2**.
(**B**) Same as (**A**), but for cell-type specific optogenetic cell body stimulation experiments for *Slc17a7::Cre* (top) and *Slc17a6::Cre* (bottom) animals infected with AAV-DIO-EF1A-ChR2-eYFP (blue) or AAV-EF1A-DIO-eYFP (green) in **Figure 5**.
(**C**) Respective placements for fiber implants (bars) and injection sites (plCoA-NAc, circles; plCoA-MeA, diamonds) in wild-type animals infected with AAV-hSyn-ChR2-mCherry (blue) or AAV-hSyn-eYFP (green) in projection-specific optogenetic axon terminal stimulation experiments in **Figure 7** and **S8**.
n denotes number of mice per group batched across 4-quad, elevated plus maze, and open field test experiments, exceeding *n* values for individual experiments due to behavioral cohort design (see STAR Methods). Relevant regions are highlighted in grey and outlined: plCoA (red), NAc (purple, only in **C**), and MeA (pink, only in **C**). All mouse brain sections reproduced from Paxinos and Franklin, 5th Edition, and numbers below all images denote its anterior-posterior distance from bregma in this atlas.[36] All scale bars, 500 μm.

Figure S3

SUPPLEMENTAL FIG 2
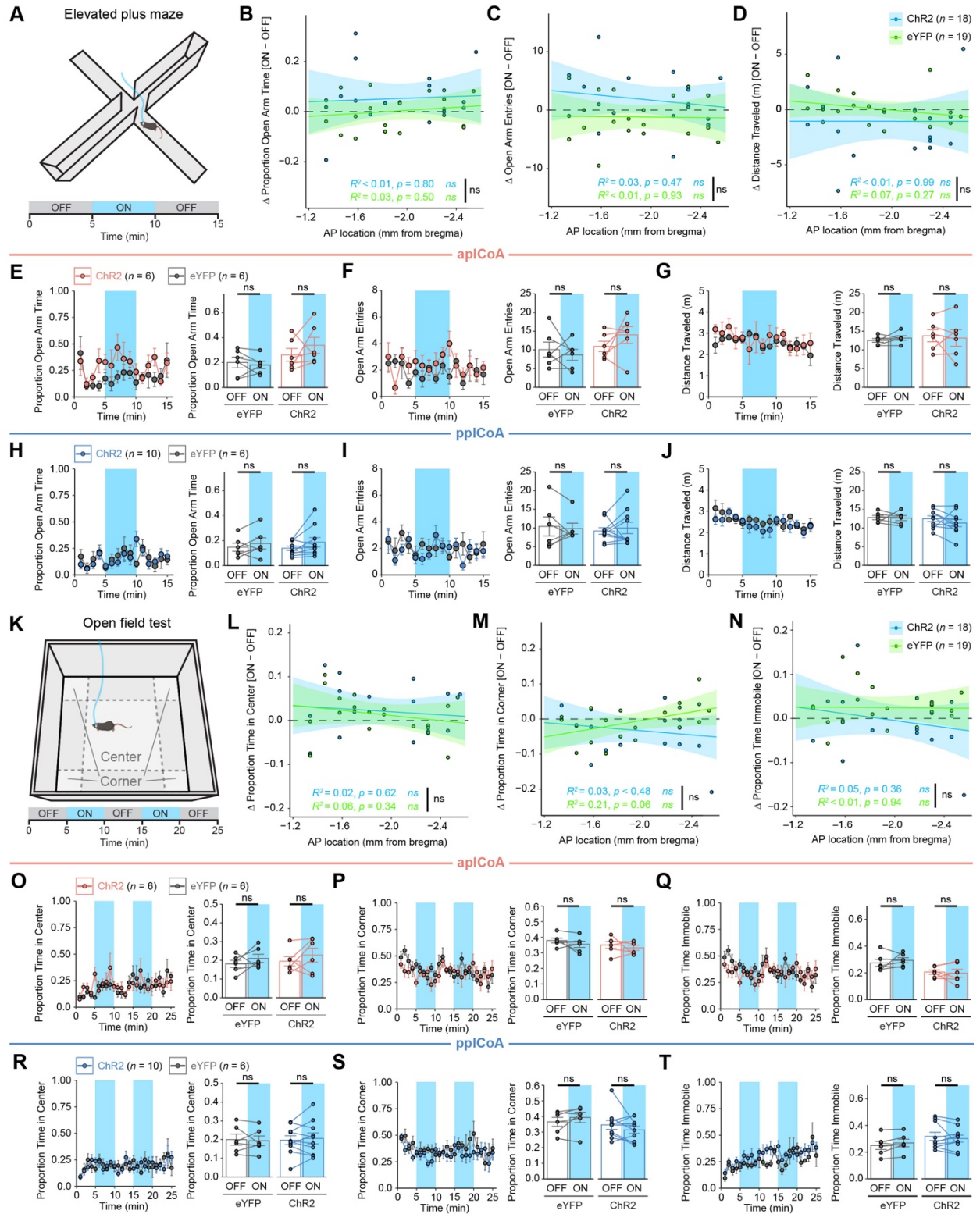
Figure S3. Behavioral effects of topographic pICoA stimulation are limited to valence alone. Related to **Figure 2**.

(A) Behavioral paradigm for optogenetic stimulation in the open field test.

(B-D) Optogenetic stimulation-induced change in time spent (**B**) and number of entries (**C**) into the open arms, as well as distance traveled (**D**) in the elevated plus maze is not correlated to anteroposterior axis position in pICoA.

(E-G) Effects of optogenetic stimulation of apICoA neurons in the elevated plus maze in 1 minute bins over time (left) and during off and on periods (right).Photostimulation of apICoA neurons does not induce a significant change in time spent (**E**) and number of entries (**F**) into the open arms, as well as distance traveled (**G**) in the elevated plus maze.

(H-J) Effects of optogenetic stimulation of ppICoA neurons in the elevated plus maze in 1minute bins over time (left) and during off and on periods (right). Photostimulation of ppICoA neurons does not induce a significant change in time spent (**H**) and number of entries (**I**) into the open arms, as well as distance traveled (**J**) in the elevated plus maze.

(K) Behavioral paradigm for optogenetic stimulation in the open field test.

(L-N) Optogenetic stimulation-induced change in time spent in the center (**L**) and corners (**M**), as well as distance traveled (**N**) in the open field test is not correlated to anteroposterior axis position in pICoA.

(O-Q) Effects of optogenetic stimulation of apICoA neurons in the open field test in 1 mintue time bins (left) and during off and on periods (right). Photostimulation of apICoA neurons does not induce a significant change time spent in the center (**O**) and corners (**P**), as well as distance traveled (**Q**) in the open field test.

(R-T) Effects of optogenetic stimulation of ppICoA neurons in the open field test in 1 minute time bins (left) and during off and on periods (right). Photostimulation of ppICoA neurons does not induce a significant change time spent in the center (**R**) and corners (**S**), as well as distance traveled (**T**) in the open field test.

All "ON" and "OFF" comparisons in bar graphs and linear regressions are on a per 5-minute basis. **(B-D, L-M)** Least-squares linear regression $\pm$ 95% confidence interval. Across panels: ns, not significant. Additional specific details of statistical tests can be found in Supplemental Table 1.
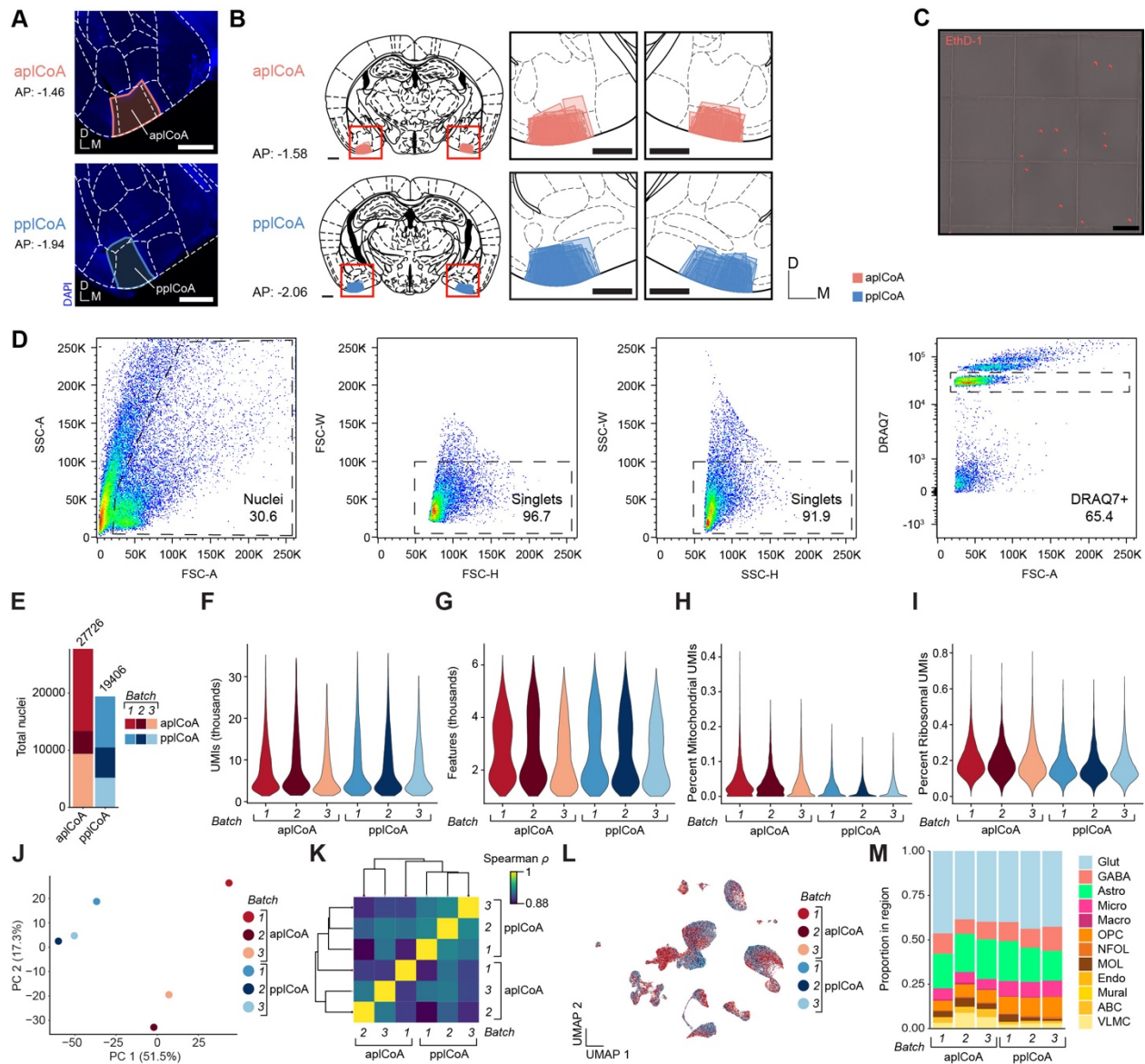
Figure S4

Figure S4. Additional information and quality-control for single-nucleus sequencing experiments. Related to **Figure 3**.

(A) Representative images of tissue microdissection sites from aplCoA and pplCoA following extraction and DAPI staining (blue). Scale bars, 500 μm.

(B) Location of all tissue sample sites for used for snRNA-seq, color coded by plCoA zone (n = 3 pools per zone, 4-11 sections per pool). Scale bars, 500 μm.

(C) Validation of nuclear enrichment after FANS. Ethidium homodimer-1 (EthD-1, red) labels nuclei on a hemocytometer after sorting, with an absence of non-nuclear, EthD-1-negative debris. Scale bar, 100 μm.

(D) Common gating strategy for FANS sorts for snRNA-seq in a representative sample.[102] Far left, morphology gate on forward and side scatter area excludes likely debris. Middle left,

forward scatter gate excludes nuclear doublets with high forward scatter width. Middle right, side scatter gate excludes nuclear multiplets with high side scatter width. Far right, stoichiometric DRAQ7+ fluorescence allows enrichment of single nuclei and exclusion of debris and multiplets.

(E) Absolute number and proportion of snRNA-seq nuclei passing quality control filters from each replicate in each plCoA zone (n = 27,726 in aplCoA, 19,406 in pplCoA, 3 libraries/batches each).

(F) Violin plot of UMIs detected per snRNA-seq nucleus for each replicate, filtered at the median per library + five times the median absolute deviation within each library (median 6081 UMIs/nucleus).

(G) Violin plot of genes detected per nucleus from each replicate, filtered at a minimum of 1000 features per nucleus (median 2547 genes/nucleus).

(H) Percent mitochondrial gene UMIs per snRNA-seq nucleus, filtered at median + five times the median absolute deviation per library (median 0.02% mitochondrial UMIs/nucleus).

(I) Percent ribosomal gene UMIs per snRNA-seq nucleus, filtered at median + five times the median absolute deviation per library (median 0.17% ribosomal UMIs/nucleus).

(J) Principal component analysis of pseudobulk snRNA-seq samples created from each batch, colored based on their combination of zone and batch identity.

(K) Evaluation of transcriptomic homology between batches, where the distance matrix is based on Spearman correlation between median expression of highly variable features for the whole dataset, and the dendrogram was created via hierarchical clustering of batches on this correlation matrix.

(L) UMAP of all snRNA-seq nuclei colored by both target region and batch identity.

(M) Relative proportion of nuclei of each type for all snRNA-seq batches.

Brain diagrams were reproduced from Paxinos and Franklin (2005).[36]
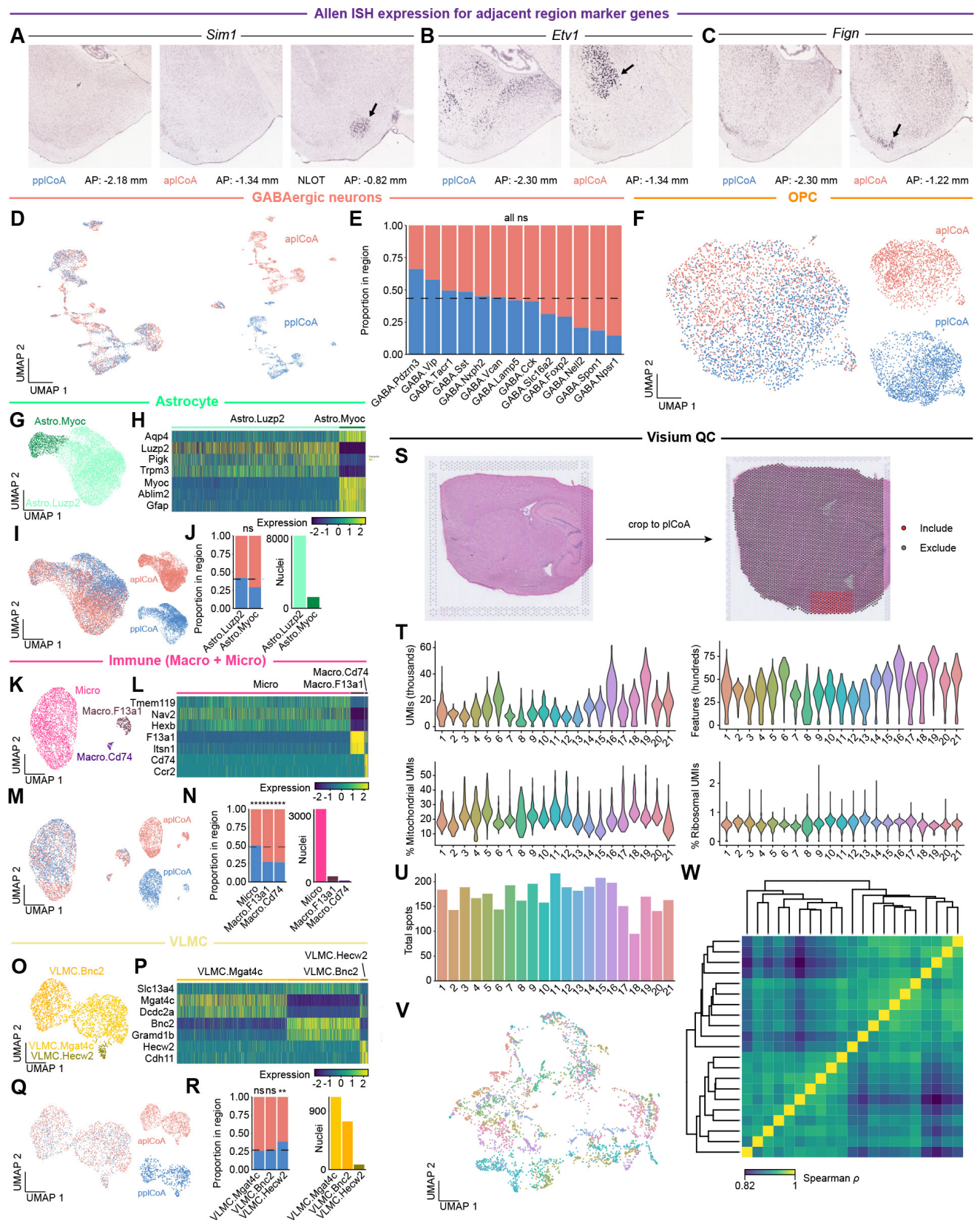
Figure S5

Figure S5. Additional information and quality control for spatial gene expression. Related to **Figure 4**.

(**A-C**) Allen ISH data for marker genes from molecular cell types adjacent to, but not within plCoA. *Sim1* (**A**) marks cells in the NLOT, *Etv1* (**B**) marks cells in the BLA and posterior basomedial amygdala, and *Fign* (**C**) marks cells in the cortex-amygdalar transition area, but none of these mark cells in the plCoA. Arrow points to respective clusters of cells marked with these genes.

(**D**) UMAP of all plCoA GABAergic neurons, colored by domain of origin.

(**E**) Relative proportion of molecular subtype nuclei from each domain within GABAergic neurons. Dotted line indicates chance level for plCoA GABAergic neuron nuclei.

(**F**) UMAP of all plCoA OPCs, colored by domain of origin.

(**G**) Two-dimensional UMAP of astrocytes, colored by molecular cell type.

(**H**) Heatmap of astrocyte subtype marker genes.

(**I**) UMAP of all plCoA astrocytes, colored by domain of origin.

(**J**) Left, relative proportion of molecular subtype nuclei from each domain within astrocytes. Dotted line indicates chance level for plCoA astrocyte nuclei. Right, relative abundance of each astrocyte subtype within plCoA.

(**K**) Two-dimensional UMAP of immune cells, colored by molecular cell type.

(**L**) Heatmap of immune cell subtype marker genes.

(**M**) UMAP of all plCoA immune cells, colored by domain of origin.

(**N**) Left, relative proportion of molecular subtype nuclei from each domain within immune cells. Dotted line indicates chance level for plCoA immune cell nuclei. Right, relative abundance of each immune cell type within plCoA.

(**O**) Two-dimensional UMAP of VLMC nuclei, colored by molecular cell type.

(**P**) Heatmap of VLMC subtype marker genes.

(**Q**) UMAP of all plCoA VLMC nuclei, colored by domain of origin.

(**R**) Left, relative proportion of molecular subtype nuclei from each domain within VLMCs. Dotted line indicates chance level for plCoA VLMC nuclei. Right, relative abundance of each VLMC subtype within plCoA.

(**S**) Left, representative section on a Visium slide capture area stained with hematoxylin and eosin. Right, representative section with capture spots overlaid (grey) and plCoA-overlapping spots highlighted (red).

(**T**) Violin plots of quality metrics for individual Visium sections on a per-spot basis in plCoA-overlapping spots (*N* = 21 sections). Upper left, UMIs per spot; upper right, features per spot; lower left, proportion mitochondrial UMIs per spot; lower right, proportion ribosomal UMIs per spot.

(**U**) Number of plCoA-overlapping capture spots per section (*n* = 3,616 total spots).

(**V**) Two-dimensional UMAP of all plCoA-overlapping capture spots, colored by section of origin.

(**W**) Evaluation of transcriptomic homology between sections, where the distance matrix is based on Spearman correlation between median expression of highly variable features for the whole dataset, and the dendrogram was created via hierarchical clustering of sections on this correlation matrix.

Across panels: ** $p < 0.01$; *** $p < 0.001$; ns, not significant. Additional specific details of statistical tests can be found in Supplemental Table 1.
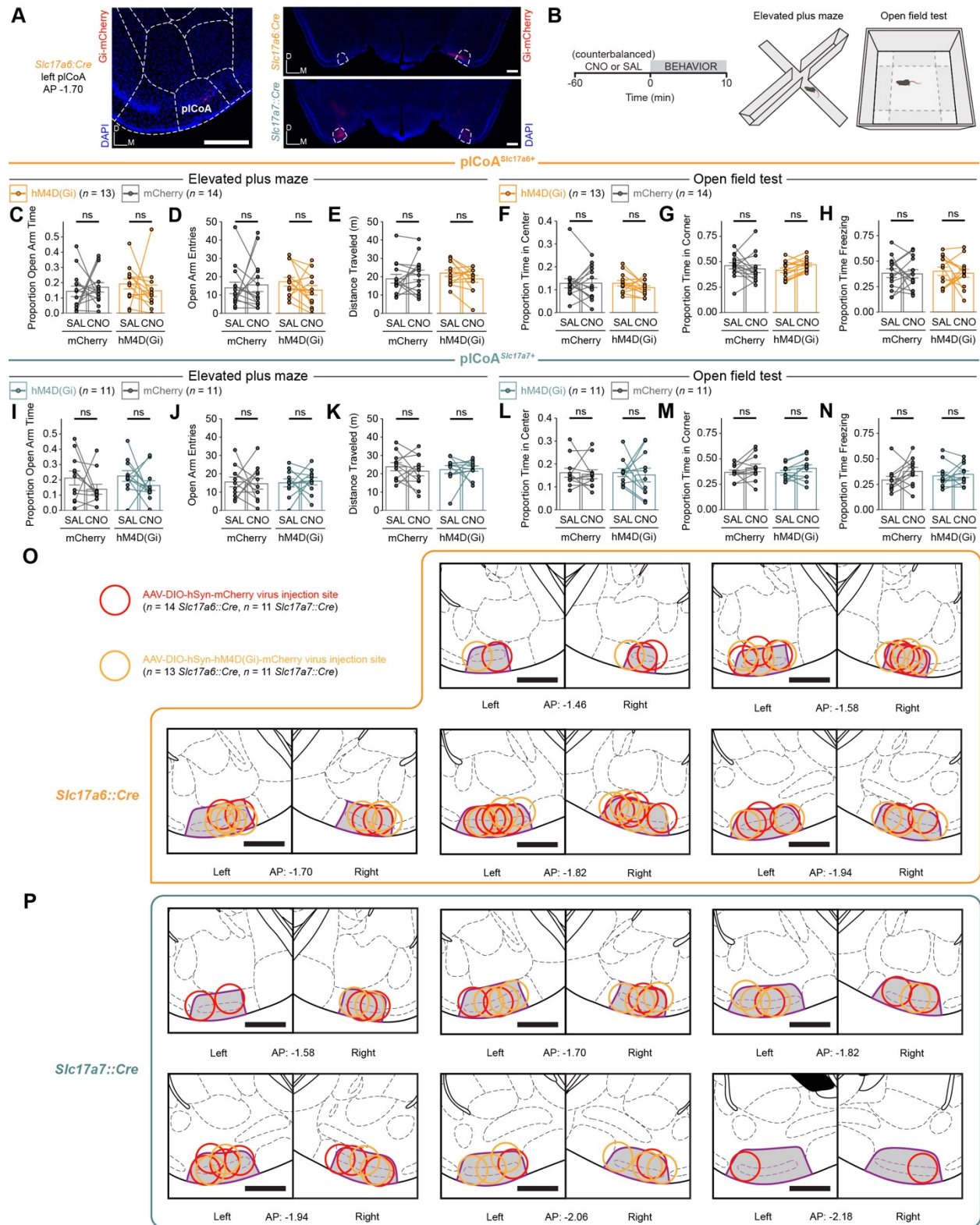
Figure S6

Figure S6. Additional information for Cre-dependent molecularly targeted chemogenetic inhibition experiments. Related to **Figure 5**.

(A) Representative histology for inhibition experiments for AAV-hM4D(Gi)-mCherry-infected *Slc17a6::Cre* (left) or *Slc17a7::Cre* (right) animals.

(B) Strategy for chemogenetic inhibition in the open field test and elevated plus maze.

(C-E) Effect of chemogenetic inhibition of plCoA$^{Slc17a6+}$ neurons in the elevated plus maze. Inhibition does not induce a significant change in time spent (**C**) or number of entries (**D**) into the open arms, as well as distance traveled (**E**) in the elevated plus maze.

(F-H) Effect of chemogenetic inhibition of plCoA$^{Slc17a6+}$ neurons in the open field test. Inhibition does not induce a significant change in time spent in the center (**F**) or corners (**G**), as well as distance traveled (**H**) in the open field test.

(I-K) Effect of chemogenetic inhibition of plCoA$^{Slc17a7+}$ neurons in the elevated plus maze. Inhibition does not induce a significant change in time spent (**I**) and number of entries (**J**) into the open arms, as well as distance traveled (**K**) in the elevated plus maze.

(L-N) Effect of chemogenetic inhibition of plCoA$^{Slc17a7+}$ neurons in the open field test. Inhibition does not induce a significant change in time spent in the center (**L**) or corners (**M**), as well as distance traveled (**N**) in the open field test.

(**O**) Histologically verified placements for viral injection sites in *Slc17a6::Cre* animals infected with AAV-DIO-hSyn-mCherry (red) or AAV-DIO-hSyn-hM4D(Gi) (light orange) in molecularly targeted chemogenetic inhibition experiments.

(**P**) Same as (**O**), but in *Slc17a7::Cre* animals.

n denotes number of mice per group batched across 4-quad, elevated plus maze, and open field test experiments, exceeding *n* values for individual experiments due to behavioral cohort design (see STAR Methods). All mouse brain sections reproduced from Paxinos and Franklin, 5th Edition, with plCoA highlighted in grey and outlined in purple, and numbers below all images denote its anterior-posterior distance from bregma in this atlas.[36] All scale bars, 500 µm. Across panels: ns, not significant. Additional specific details of statistical tests can be found in Supplemental Table 1.
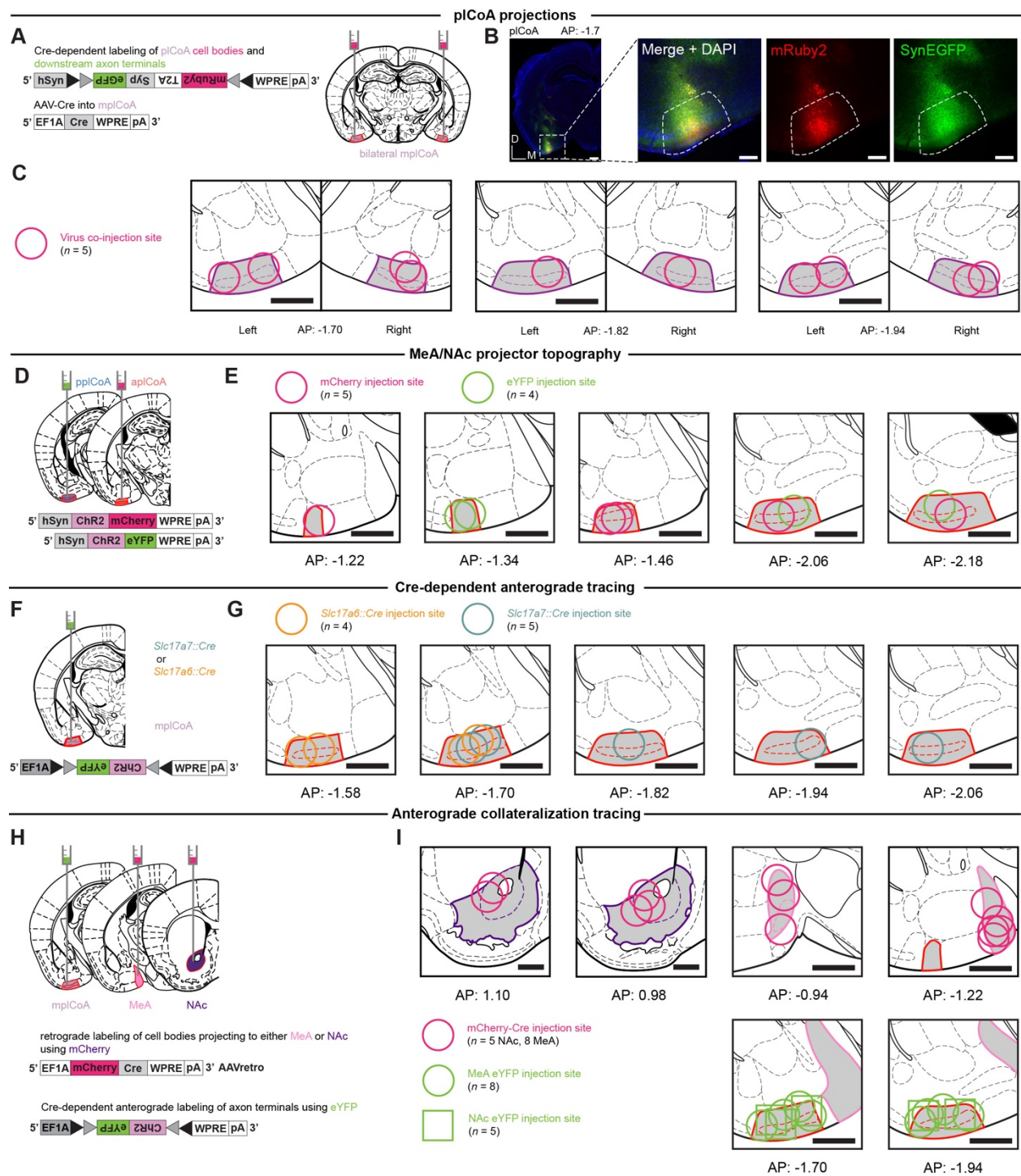
Figure S7

Figure S7. Additional information for plCoA anterograde tracing experiments. Related to **Figure 6**.

(A) Schematic for general anterograde output mapping strategy, where a virus labeling cell bodies in plCoA with mRuby and presynaptic terminals in downstream regions with synaptophysin-bound eYFP.

(B) Histological image of plCoA injection site in a representative animal. Scale bar, 200 µm.

(C) Histologically verified placements for viral injection sites in initial anterograde tracing experiments.

(D) Schematic for dual-color topographic anterograde tracing: two counterbalanced fluorophores were injected into aplCoA and pplCoA, and each color was quantified in major projection targets of plCoA.

(E) Histologically verified placements for viral injection sites in dual-color anterograde tracing experiments.

(F) Schematic for Cre-dependent anterograde output mapping strategy: a Cre-dependent virus expressing eYFP was injected into either an *Slc17a6::Cre* or *Slc17a7::Cre* animal to determine relative output enrichment for either broad cell type.

(G) Histologically verified placements for viral injection sites in Cre-dependent molecular anterograde tracing experiments.

(H) Schematic of anterograde viral strategy to explore collateralization of plCoA MeA and NAc projection neurons to other regions.

(I) Histologically verified placements for viral injection sites in collateralization experiments. Relevant regions are highlighted in grey and outlined: plCoA (red), NAc (purple, only in **I**), and MeA (pink, only in **I**). All mouse brain sections reproduced from Paxinos and Franklin, 5th Edition, and numbers below all images denote its anterior-posterior distance from bregma in this atlas.[36] All scale bars 500 µm unless noted elsewhere.
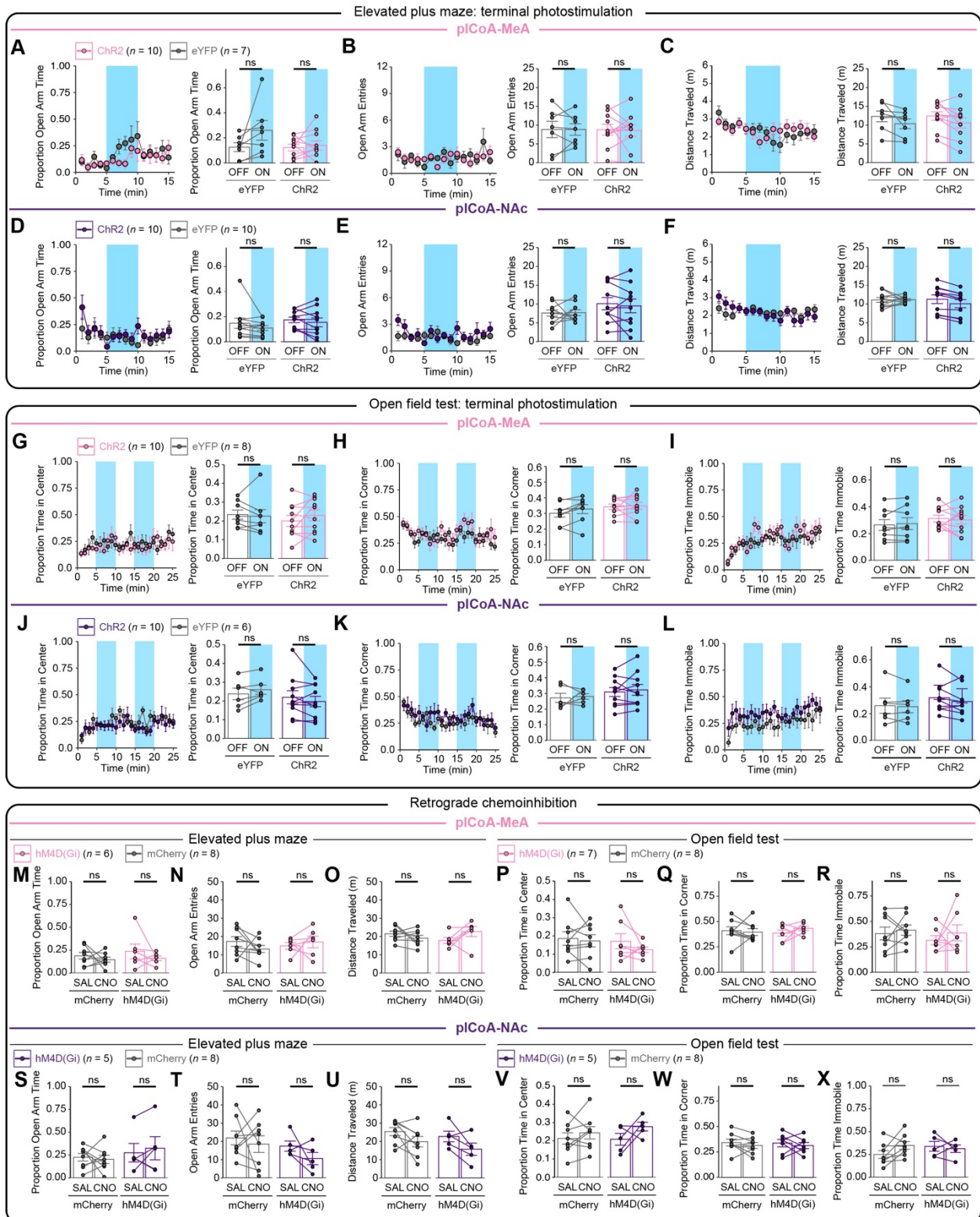
Figure S8

Figure S8. Manipulation of plCoA projections to MeA or NAc in either direction does not change features of behavior unrelated to innate valence. Related to **Figure 7**.
(A-C) Effects of optogenetic stimulation of plCoA terminals in MeA in the elevated plus maze in time bins of 1 minute (left) and during off and on periods (right). Photostimulation does not induce a significant change in time spent (**A**) and number of entries (**B**) into the open arms, as well as distance traveled (**C**) in the elevated plus maze.
(D-F) Effects of optogenetic stimulation of plCoA terminals in NAc in the elevated plus maze in time bins of 1 minute (left) and during off and on periods (right). Photostimulation does not induce a significant change in time spent (**H**) and number of entries (**I**) into the open arms, as well as distance traveled (**J**) in the elevated plus maze.
(G-I) Effects of optogenetic stimulation of plCoA terminals in MeA in the open field test in time bins of 1 minute (left) and during off and on periods (right). Photostimulation does not induce a significant change time spent in the center (**G**) and corners (**H**), as well as distance traveled (**I**) in the open field test.
(J-L) Effects of optogenetic stimulation of plCoA terminals in NAc in the open field test in time bins of 1 minute (left) and during off and on periods (right). Photostimulation does not induce a significant change time spent in the center (**G**) and corners (**H**), as well as distance traveled (**I**) in the open field test.
(**M-O**) Effects of chemogenetic inhibition of plCoA-MeA projection neurons in the elevated plus maze. Inhibition does not induce a significant change in time spent (**M**) and number of entries (**N**) into the open arms, as well as distance traveled (**O**) in the elevated plus maze.
(**P-R**) Effects of chemogenetic inhibition of plCoA-MeA projection neurons in the open field test. Inhibition does not induce a significant change in time spent in the center (**P**) and corners (**Q**), as well as distance traveled (**R**) in the open field test.
(**S-U**) Effects of chemogenetic inhibition of plCoA-NAc projection neurons in the elevated plus maze. Inhibition does not induce a significant change in time spent (**S**) and number of entries (**T**) into the open arms, as well as distance traveled (**U**) in the elevated plus maze.
(**V-X**) Effects of chemogenetic inhibition of plCoA-NAc projection neurons in the open field test. Inhibition does not induce a significant change in time spent in the center (**V**) and corners (**W**), as well as distance traveled (**X**) in the open field test.
Across panels: ns, not significant. Additional specific details of statistical tests can be found in Supplemental Table 1.